Morphology of ABC Triblock Copolymers

Wei Zheng

Division of Physics, Mathematics and Astronomy, California Institute of Technology, Pasadena, California 91125

Zhen-Gang Wang*

Division of Chemistry and Chemical Engineering, California Institute of Technology, Pasadena, California 91125

Received April 10, 1995; Revised Manuscript Received July 17, 1995®

ABSTRACT: We present results from theoretical calculations of the morphological phase diagrams for ABC triblock copolymers in the strong segregation limit. The chain conformation free energy is approximated following an approach proposed by Ohta and Kawasaki. Our study focuses on two unique features of the ABC triblock copolymers, namely, the dependence of the morphology on the sequence of the triblock chain and the relative strength of the various interaction parameters. Our results compare favorably with experimental observations. In addition, we predict the existence of some new structures that have yet to be observed experimentally.

I. Introduction

Block copolymers have received considerable attention, both experimentally and theoretically, due to their fascinating ability to self-assemble into a variety of ordered nanoscale morphologies. Recently, self-assembled ordered structures with periodicities on the nanometer scale have become an important area of study because of their applications in nanotechnology. For instance, it has been suggested that block copolymers can be used in the development of new classes of electronic devices[1,2] and in the synthesis of mesoporous solids, which can be used as catalysts and sorption media.[3,4] One of the distinct advantages of block copolymers is the controllability of the size and morphology of the nanostructures by changing the molecular weight, molecular architecture, and composition of the copolymers.

Ordered morphologies and phase transitions in linear AB-type diblock copolymers have been studied for many years. Helfand et al.,[5] Semenov,[6] and Ohta and Kawasaki[7,8] developed approaches for studying the strong segregation limit, while Leibler studied the weak segregation limit by using an order parameter Landau mean-field theory.[9] Fredrickson and Helfand[10] incorporated the effects of concentration fluctuations in the order–disorder transition by reducing the effective Hamiltonian of block copolymers to a form previously studied by Brazovskii.[11] Noolandi et al. developed a self-consistent mean-field theory for studying both the strong and weak segregation limits.[12] Recently, Melenkevitz and Muthukumar,[13] Muthukumar,[14] Matsen and Schick,[15] and Olmsted and Milner[16] have made important contributions to the further development of theory of diblock copolymers.

It is now well recognized that the phase behavior of AB diblock copolymers is determined by three factors: the overall degree of polymerization, $N = N_A + N_B$; the composition of the copolymer characterized by $f = N_A/N$; and the temperature expressed in terms of the Flory–Huggins interaction parameter χ. For symmetric diblocks ($f = 0.5$), an order–disorder transition takes place at $\chi N \sim 10$.[9] Depending on the composition and/or temperature, body-centered cubic (bcc) ordered spheres, hexagonally ordered cylinders, lamellae, and more complex bicontinuous structures have been obtained below the order–disorder transition temperature.[17]

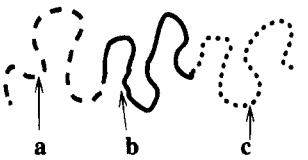

Figure 1. Schematic representation of ABC triblock copolymer. For a given sequence, we use a and c to denote the end blocks and b to denote the center block.

While the equilibrium morphologies of AB diblock copolymers have been relatively well understood theoretically (except for some uncertainties with regard to the bicontinuous phases[16,18–20]), considerably less theoretical work exists for the ABC type triblock copolymers.[21–24] The recent experimental discovery of exotic new morphologies in ABC triblocks and a growing interest in using these copolymers to synthesize new nanoscale structures have increased the need for a theoretical study of these systems.

ABC triblock copolymers consist of three different polymer segments A, B, and C, that are chemically bonded together, as illustrated in Figure 1. Since there are three interaction parameters, χ_{AB}, χ_{BC}, and χ_{CA}, in ABC triblock copolymers, as opposed to one interaction parameter, χ_{AB}, in AB diblock copolymers, the microphase separation of ABC triblock copolymers is much more complicated than that in diblock copolymers. More importantly, some distinctively new features arise in triblock copolymers that are absent in the diblock counterpart. For example, the morphological structure of triblock copolymers depends not only on the temperature, the overall molecular weight, and the fraction of each block but also crucially on the sequence of the blocks in the chain (i.e., whether it is sequenced A–B–C, B–C–A, or C–A–B). Indeed, recent experiments have shown that the lamellar morphology is formed in the system of poly(isoprene-*b*-styrene-*b*-2-vinylpyridine) (ISP) with volume fraction 1:1:1,[25] whereas the hexagonally ordered coaxial cylinder phase is obtained in the system of SIP with the same composition.[26] The sche-

® Abstract published in *Advance ACS Abstracts,* September 1, 1995.

0024-9297/95/2228-7215$09.00/0

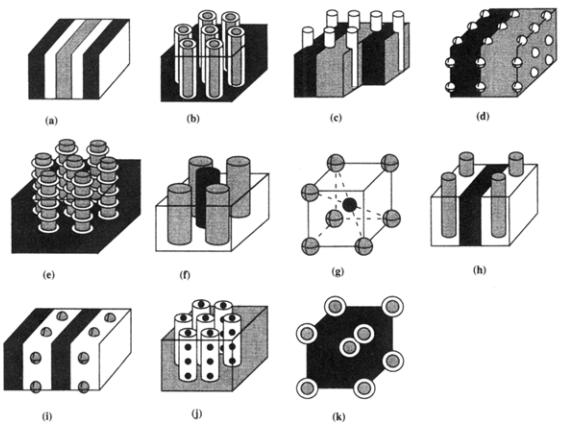

Figure 2. Schematic representation of all the phases considered. Dark, a; white, b; gray, c. (a) Lamellar phase; (b) coaxial cylinder phase; (c) lamella–cylinder phase; (d) lamella–sphere phase; (e) cylinder–ring phase; (f) cylindrical domains in a square lattice structure; (g) spherical domains in the CsCl-type structure; (h) lamella–cylinder–II; (i) lamella–sphere–II; (j) cylinder–sphere; (k) cocentric spherical domain in the bcc structure.

matic representations of the lamellar phase and the coaxial cylinder phase are shown in parts a and b of Figure 2, respectively.

Even for a given sequence, say A–B–C, one can obtain different morphologies, depending on the relative magnitudes of the three Flory–Huggins parameters and the composition. Thus, richer and more complex morphological behaviors are expected in ABC triblock copolymers than in AB diblocks. In addition to the discovery of ordered spherical, cylindrical, lamellar, and ordered tricontinuous double-diamond structures (OTDD),[25–27] which bear the same basic structural features as the corresponding structures in AB diblock copolymers, several intriguing new morphologies have been reported in recent experiments. Auschra et al.[28,29] demonstrated the formation of three new phases: a lamella–cylinder combination phase, a lamella–sphere combination phase, and a cylinder–ring combination phase. The schematic representations of the three new phases are given in parts c–e, Figure 2, respectively. The possibility of forming morphologies which are a combination of the lamellar, cylinder, and sphere phases in triblock copolymers was first predicted by Riess et al.[22,23] These combination morphologies, which often have characteristics of one-, two-, and three-dimensional order simultaneously, can have unique mechanical properties. Nanostructures templated after these morphologies are also expected to have unusual electronic and transport properties.

Considering the novel features which are alluded to above, we feel that the study of triblock copolymers represents a significantly new direction in self-assembling polymers. In this paper, we map out the three-component phase diagrams of ABC triblock copolymers in the entire range of f_A, f_B, and f_C in the strong segregation limit by applying a simple, approximate theory put forth by Ohta, Kawasaki, and Nakazawa[7,8,21] to the most general cases in which χ_{AB}, χ_{BC}, and χ_{CA} are not necessarily equal to each other. By varying the interaction parameters and the composition of copolymers, we seek to establish a relationship between the molecular characteristics of the system and its morphologies.

The key simplification in the Ohta and Kawasaki theory is the separation of the free energy of the copolymer system into a short-range interaction, which accounts for the interfacial free energy of the system, and a long-range interaction, which accounts for the chain conformation energy. In addition, these authors assume that the long-range interaction can be approximated by a term proportional to $1/k^2$, as suggested by the small k behavior of the structure factor calculated in the random-phase approximation. A similar approximation was proposed by Stillinger[30] in his study of micellar self-assembly. Although the validity of this last assumption is difficult to justify theoretically, previous results of Ohta and Kawasaki,[7] Nakazawa and Ohta,[21] and Muthukumar and Melenkevitz[13] on block copolymers and of Stillinger[30] and Chandler and coworkers[31] on short surfactant systems suggest that such a representation seems to be capable of capturing many of the essential features of the microphase separation of block copolymer systems. Here we adopt this approximate approach for its simplicity in implementation. More accurate approaches, such as the method of electrostatic analogy developed by Semenov[6] and the "wedge" approach developed by Milner and Olmsted,[16] can be employed, in principle, as demonstrated in the recent work of Kane and Spontak,[32] who has extended Semenov's approach to the strongly-segregated lamellar phase of ABC triblock copolymers; however, extensive computational efforts will be required if these methods are to be applied to the complicated morphologies studied in this paper. Although the results presented herein are subject to the inherent approximation in the approach and hence may not be quantitatively accurate, we believe that the features of the phase diagrams presented can be useful in providing a guide for further experimental and theoretical studies. More precise results can be obtained by the self-consistent method.

The organization of the paper is as follows: In section II, we discuss the general formulation of the free energy of a triblock copolymer system, by following the Ohta–Kawasaki approach. In section III, we present and discuss phase diagrams of triblock copolymer systems; these phase diagrams are classified according to the relative strength of the interaction parameters. In section IV, we compare our calculations with some available experimental results. Section V is the conclusion. The Appendix contains a detailed calculation of the free energy of a lamella–sphere phase, which illustrates the method we employed.

II. Model and Free Energy

We consider a model system containing n monodisperse triblock copolymer chains with an overall degree of polymerization N. Each chain consists of three types of monomers, a, b, and c, with interaction parameters χ_{ab}, χ_{bc}, and χ_{ac}. Henceforth, we will use the lower-case "a", "b", and "c" to designate the segmental position of the three blocks such that "a" and "c" are the outer blocks while "b" is the middle block. The upper-case letters refer to the chemical makeup of the blocks. Thus, we will always designate a triblock copolymer as a–b–c, even though there can be three chemically distinct sequences A–B–C, B–C–A, and B–A–C. For the sake of simplicity, we will assume that all three blocks have the same Kuhn statistical segment length, which we take to be unity, and the same monomeric volume v_0. The volume fraction of blocks a, b, and c in a chain are f_a, f_b, and f_c, respectively, which satisfy $f_a + f_b + f_c = 1$. We assume that the system is incompressible.

In the strong segregation limit, the microdomains form a regular arrangement, giving rise to periodic structures with the interfacial width much smaller than the lattice dimensions. The free energy of the system can be separated into two parts: an entropic chain-conformational free energy, and an interfacial free energy, whose strength is characterized by the Flory–Huggins parameters. We define a characteristic length scale (or one of the characteristic length scales) of a periodic structure to be l. For example, l can be the period in the lamellar phase, the lattice constant of the square lattice in the cylinder phase, or one of the periods in the lamella–cylinder phase.

The free energy per chain can be written as

$$F = \frac{l^2}{2N}\Phi(f_a,f_c) + \frac{\sigma_{av}Nv_0}{l} \tag{1}$$

where $\Phi(f_a,f_c)$ is a scaling function which depends on the morphology of the system, v_0 is the volume of a monomer, and σ_{av} is an average interfacial tension to be explained later.

While eq 1 is formally exact in the strong segregation limit, further progress requires an explicit expression for the scaling function $\Phi(f_a,f_c)$. Here we use the approximation suggested by Nakazawa and Ohta.[21] In this approximation, $\Phi(f_a,f_c)$ is calculated from the asymptotic behavior of the structure factor in the long-wavelength limit. More specifically, $\Phi(f_a,f_c)$ is written as

$$\Phi(ff_c) = \sum_{\alpha\beta=a,c}\sum_{\hat{Q}}\frac{1}{\hat{Q}^2}A_L^{\alpha\beta}(f_a,f_c)\,\Psi_\alpha(\hat{Q})\,\Psi_\beta^*(\hat{Q}) \tag{2}$$

where $\Psi_\alpha(\hat{Q})$ is the Fourier transform of $\Psi_\alpha(\vec{r})$, which is the local volume fraction deviation of monomers α from its uniform distribution, i.e.

$$\Psi_\alpha(\hat{Q}) = \frac{1}{V_{cell}}\int d\vec{r}\;\Psi_\alpha(\vec{r})\exp(i\vec{Q}\vec{r}) \tag{3}$$

with V_{cell} being the volume of the unit cell. The quantity $\hat{Q}$ is the reciprocal lattice vector scaled by l, i.e., $\hat{Q} = Ql$. In eq 2, $\Psi_b(\hat{Q})$ has been eliminated by the use of incompressibility. The coefficient $A_L^{\alpha\beta}(f_a,f_c)$ is given by

$$A_L^{aa} = B\frac{2(1-f_c)^2}{f_a^2} \tag{4}$$

$$A_L^{ac} = A_L^{ca} = B\frac{1-f_a^2-f_c^2}{f_af_c} \tag{5}$$

$$A_L^{cc} = B\frac{2(1-f_a)^2}{f_c^2} \tag{6}$$

with

$$B = \frac{6}{\{3-2(f_a+f_c)-(f_a-f_c)^2\}(1-f_a-f_c)^2} \tag{7}$$

The average interfacial tension is given by

$$\sigma_{av} = \sum_{\alpha\beta=a,b,c}\hat{S}_{\alpha\beta}\sigma_{\alpha\beta}/\hat{V}_{cell} \tag{8}$$

where $\hat{V}_{cell}$ is the volume of the unit cell scaled by l^3, and $\hat{S}_{\alpha\beta}$ is the interfacial area between α and β domains in a unit cell scaled by l^2. If there is more than one disconnected interface between the α and β domains in a unit cell, the interfacial area is the sum of all the disconnected interfacial areas. The variable $\sigma_{\alpha\beta}$ is the interfacial tension between the α and β domains. In the strong segregation limit, if we ignore the presence of the third component in the interfacial region between α and β, $\sigma_{\alpha\beta}$ is proportional to $\chi_{\alpha\beta}^{1/2}$ and independent of the block ratio.[8,33]

Minimization of F with respect to l yields the length scale l^* and the corresponding free energy F^*

$$l^* = [\sigma_{av}N^2v_0/\Phi(f_a,f_c)]^{1/3} \tag{9}$$

$$F^* = C^*[\hat{\sigma}_{av}{}^2\Phi(f_a,f_c)]^{1/3} \tag{10}$$

where $C^* = 3(\sigma_{ab}{}^2v_0{}^2N/2)^{1/3}$ is the free energy of a three-phase, four-layer lamellar phase (see Figure 2a), with interfacial tension $\sigma_{ab} = \sigma_{bc}$, and

$$\hat{\sigma}_{av} = \frac{1}{2}[\hat{S}_{ab} + \hat{S}_{bc}(\sigma_{bc}/\sigma_{ab}) + \hat{S}_{ac}(\sigma_{ac}/\sigma_{ab})]/\hat{V}_{cell} \tag{11}$$

Thus, the equilibrium state of the system, which is determined by the minimum value of F, depends on the relative strength of interfacial tensions σ_{bc}/σ_{ab} and σ_{ac}/σ_{ab}, in addition to the composition.

For some simple morphologies such as the lamellar, cylinder, and spherical phases, where there is only one characteristic length, the obtained F^* is the minimum free energy of the morphology. However, for the more complex morphologies such as the lamellar–cylinder phase in which there are two characteristic length scales, F^* depends on the ratio of the two length scales through $\Phi(f_a,f_c)$ and $\hat{\sigma}_{av}$, and the minimum free energy is obtained by further minimization of F^* with respect to this ratio. The detailed calculation of the free energy of the lamella–cylinder phase is presented in the Appendix; the calculation of the free energies of the other morphologies is carried out in a similar fashion. Although of great current interest, we do not consider the ordered tricontinuous phases in this paper. Our preliminary analysis shows that the ordered tricontinuous phases in triblocks are much more complex and subtle than the corresponding bicontinuous phases in diblocks. Furthermore, even for diblocks, there is controversy as to the stability of these phases in the strong segregation limit.[16,18–20]

III. Phase Diagrams of ABC Triblock Copolymers

Three different types of homopolymers A, B, and C, with interaction parameters χ_{AB}, χ_{BC}, and χ_{CA}, can be bonded together to form A–B–C, A–C–B, or B–C–A copolymers. If χ_{AB}, χ_{BC}, and χ_{CA} are not equal to one another, the different sequences will have different phase behaviors. For a system with a given sequence and volume fractions, using "a", "b", and "c" to label the three blocks as explained in section II, we determine the equilibrium phase diagrams in terms of the ratios of the interfacial tensions σ_{ac}/σ_{ab} and σ_{bc}/σ_{ab}. For convenience, we assume that $\sigma_{ab} \le \sigma_{bc}$. If the opposite is true, we may always relabel the blocks such that $\sigma_{ab} \le \sigma_{bc}$. We define $\gamma_2 = \sigma_{ac}/\sigma_{ab}$ and $\gamma_1 = \sigma_{bc}/\sigma_{ab}$. The a–b–c triblock copolymer systems can be classified into six classes according to the relative strength of the interfacial tensions γ_1 and γ_2, as shown in Table 1.

Table 1

(1) $\gamma_1 = 1, \gamma_2 < 1$	(2) $\gamma_1 = 1, \gamma_2 = 1$	(3) $\gamma_1 = 1, \gamma_2 > 1$
(4) $\gamma_1 > 1, \gamma_2 < 1$	(5) $\gamma_1 > \gamma_2 > 1$	(6) $\gamma_2 > \gamma_1 > 1$

Once the relative strength of the interaction parameters is specified, the morphology is uniquely determined by the composition of the system.

A. Variation of Morphologies with Composition. In this section, we focus on the variation of morphologies with composition. To this end, we set $\gamma_1 = \gamma_2 = 1$. The three-component triangle phase diagram is shown in Figure 3a. The increment of the volume fractions f_a, f_b, and f_c in the phase diagram is 0.1. At each grid point of the phase diagram, the free energies of all the morphologies listed in Figure 2 are calculated and the equilibrium state is determined by the morphology with the lowest free energy. From Figure 3a, it is evident that, with an increasing value of f_b, the equilibrium morphology of the system changes from the lamellar structure to the cylindrical domains in the square lattice structure and finally to the spherical domains in the CsCl-type structure. Their schematic representations are shown in parts a, f, and g of Figure 2, respectively. When $f_a = f_c$, the free energies of spherical, cylindrical, and lamellar phases are as shown in Figure 3b, a result consistent with that of Nakazawa and Ohta.[21]

Near the edge of the triangle phase diagram, where at least one of the three components f_a, f_b, and f_c is less than 0.1, other morphologies are possible, although these are not shown in Figure 3a. At the edge ac of the triangle phase diagram where $f_b \leq 0.1$, we find several other phases competing for stability in addition to the stable lamellar phase. For $f_b = 0.1$ and $f_a \simeq f_c$, the free energies of the lamella–cylinder and lamellar–sphere phases are very close to that of the lamellar phase. Their schematic representations are shown in parts c and d of Figure 2. The free energies of the lamellar, lamellar–cylinder, and lamellar–sphere phases, for $f_a = f_c$, are shown in Figure 3c. The free energy of the lamellar–cylinder phase is lowest for $0.025 < f_b < 0.1$, and that of the lamellar–sphere phase is lowest for $f_b < 0.025$. In the lamellar–cylinder or lamellar–sphere phases, the minority species b blocks form cylindrical or spherical domains along the a/c lamellar interface, rather than flat layers in the lamellar phase. By reducing the interfacial area of a/b and b/c interfaces, the interfacial energy is reduced so that the total free energy is lowered. Although f_b must be quite small to form the lamella–cylinder and lamella–sphere phases in this case, we will show later that when the value of γ_2, the interfacial tension between the two outer blocks a and c, is reduced in comparison to the interfacial tension between the center block and the outer blocks, these phases can form at much larger values of f_b.

At the other two edges of the triangle phase diagram, i.e., ab (or bc), where the volume fraction of one of the two end blocks f_c (or f_a) is very small and $f_a \sim f_b$ (or $f_c \sim f_b$), two other morphologies compete for stability with the lamellar phase. One of these phases is demonstrated in Figure 2h; we call this phase the lamella–cylinder–II phase. In this phase, the minority species, say a, forms cylindrical domains located regularly inside the b domains of the b/c lamellar stacking. Another morphology is shown in Figure 2i; we call this phase the lamella–sphere–II phase. In this case, the minority species a forms spheres located hexagonally inside of b domains, with blocks b and c forming a lamellar structure. Although these two morphologies have an appearance similar to the previously studied lamella–

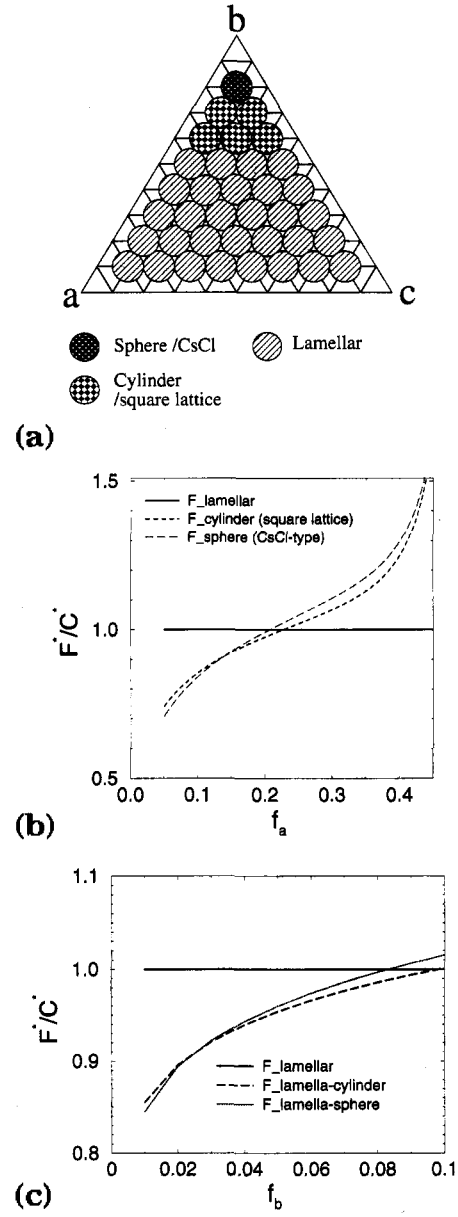

Figure 3. (a) Phase diagram for $\gamma_1 = 1.0$ and $\gamma_2 = 1.0$. (b) Equilibrium free energy F^*/C^* for lamellar, cylindrical, and spherical structures for $f_a = f_c$, $\gamma_1 = 1.0$, and $\gamma_2 = 1.0$. (c) Equilibrium free energy F^*/C^* for the lamellar, lamella–cylinder, lamella–sphere phases for $\gamma_1 = 1.0$ and $\gamma_2 = 1.0$.

cylinder and lamella–sphere phases, respectively, they are different structures. The cylindrical or spherical domains in the lamella–cylinder–II or lamella–sphere–II phases, respectively, are formed by one of the outer blocks and are located inside the domains formed by the center blocks, while the cylindrical domains and spherical domains in the lamella–cylinder and the lamella–sphere phases, respectively, are formed by the center blocks and located at the interface of the two outer blocks. The lamella–cylinder–II phase becomes stable when $f_a < 0.016$ at $f_b = f_c = 0.492$, whereas the lamella–sphere–II phase is always nearly stable even when $f_a < 10^{-6}$. The stability of both morphologies can be enhanced when the surface tension γ_1 is decreased. We are not yet aware of any experiments which show these new phases.

At the a or c corner of the phase diagram, where f_b and f_c, or f_b and f_a, respectively, are very small, our calculations show that the coaxial cylinder and cylinder–sphere phases are nearly stable. In the coaxial cylinder

phase, the minority species, say c, form inner cylinders, blocks b form the shells around these cylinders, and blocks a form the matrix. In the cylinder–sphere phase, blocks c form spheres which are embedded in the cylindrical domains formed by blocks b and blocks a form the matrix. Schematic representations of these phases are shown in parts b and j of Figure 2. At $f_c, f_b = 0.1, 0.1$ (or $f_a, f_b = 0.1, 0.1$), the free energy ratios $F_{\text{coaxial cylinder}}/F_{\text{lamellar}} = 1.026$ and $F_{\text{cylinder-sphere}}/F_{\text{lamellar}} = 1.060$. However, the coaxial cylinder phase becomes the dominant phase at $f_b \leq 0.05$ and $f_c \leq 0.05$, while the cylinder–sphere phase is always nearly stable when $\gamma_1 = 1.0$ and $\gamma_2 = 1.0$. As we will show later, the cylinder–sphere phase is stable only in the region of $f_c/f_b \ll 1.0$ when γ_1 is increased to a large value.

It should be pointed out that near the edges of the phase diagram of Figure 3a, where at least one of the volume fractions of the blocks is very small, the size of domains formed by the minority species is also very small. As the size of the domains becomes smaller, an increasing number of wave vectors are needed to obtain a given accuracy in the free energy calculation.

A more serious problem arises when one of the volume fractions f_α (α = a, b, c) becomes very small. The three edges of the triangle phase diagram are the phase diagrams of a–b, b–c, and c–a diblock copolymers where one of the three volume fractions f_c, f_a, and f_b is zero. It is well-known that diblock copolymers, in the strong segregation limit, undergo the following sequence of morphology changes as the asymmetry in the lengths increases: lamellar → hexagonal cylinders → bcc spheres. (Different theories give slightly different values of f at the transitions.[6,7]) Our calculated phase diagrams do not seem to approach the corresponding diblock phase diagrams as one of the volume fractions vanishes. There are two reasons for this discrepancy. The first reason is that we have used a rather coarse grid (f_α changes by an increment of 0.1). The second, and more fundamental, reason is the assumption of strong segregation. The theory that we employ assumes strong segregation between all pairs in the triblock; no intermixing is allowed. This assumption clearly becomes invalid as the volume fraction of one of the blocks becomes small. Rather than forming three distinct domains containing a, b, and c components, respectively, the tiny block will become soluble in the matrix of the other two blocks. If strong segregation is insisted upon, then one does not, in general, expect the triblock phase behavior to approach the diblock phase behavior in the limit of vanishing fraction of one of the blocks. This is because, in a true diblock copolymer system, the two ends of the diblock chain are unconstrained. However, in an a–b–c triblock, the two ends of the b block are connected with the a and c blocks on either end, and, consequently, when one insists on three distinct domains consisting of the three blocks, the ends of the b blocks are always tethered, even when one of the end blocks (a or c) becomes vanishingly small. This argument leads us to conclude that the diblock phase behavior is approached only in the limit of $f_b \to 0$, but not in the limit of f_a or $f_c \to 0$.

We have performed a separate calculation using the Semenov approach on the lamellar to cylinder (the coaxial structure as shown in Figure 2b) transition and studied the shift of the phase boundary as one of the volume fractions becomes vanishingly small. Results of this calculation are consistent with the conclusion given above.[34] We have also used the Ohta–Kawasaki–

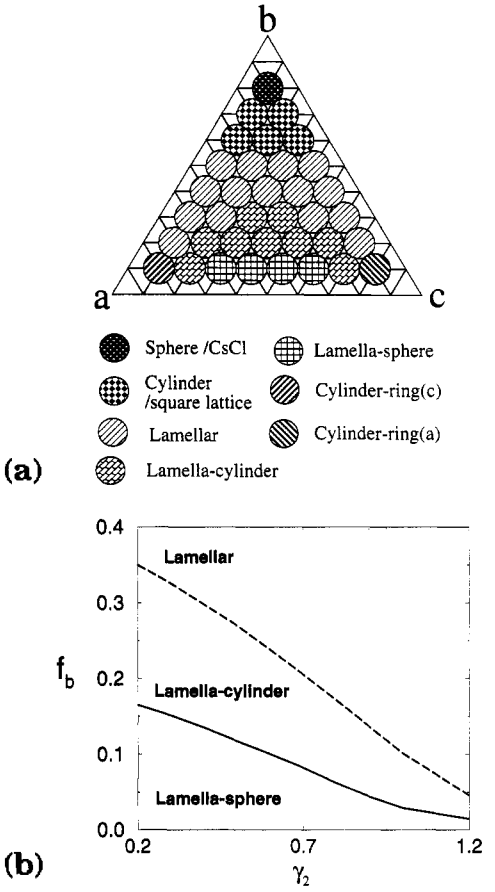

Figure 4. (a) Phase diagram for $\gamma_1 = 1.0$ and $\gamma_2 = 0.2$. (b) Phase diagram in terms of f_b versus γ_2 for a system with $f_a = f_c$ and $\gamma_1 = 1.0$.

Nakazawa approach to study the behavior of the phase diagram for decreasing f_b (below 0.1). Our results show that very close to the ac edge, the phase behavior indeed becomes qualitatively similar to the a–c diblock. Quantitative recovery of the a–c diblock behavior is not expected because of the approximate nature of the theory.

B. Effects of Interfacial Tensions. The region of morphologies which appear near the edges and corners of the triangle phase diagram in Figure 3a can be greatly enlarged when we change the relative strength of interaction parameters γ_1 and γ_2. To focus on the influence of γ_2, we set $\gamma_1 = 1$. A system can be classified into one of the three groups shown in the first row of Table 1 according to the relative strength of γ_2. In the first group, $\gamma_2 < 1$, and the interaction between the two outer blocks is more favorable than that between the center block and the two outer blocks. Consequently, there is a greater tendency to form morphologies such as the lamella–cylinder, lamella–sphere, and cylinder–ring phases, in which some parts of a/b and b/c interfaces are replaced by a/c interfaces. In the second group, the interaction between the two outer blocks is comparable to the interaction between the outer blocks and the center blocks, and morphologies with a/c interfaces can only exist in a small portion of the phase diagram, as discussed in section III.A and shown in Figure 3c. In the third group, $\gamma_2 > 1$, the interaction between the two outer blocks is less favorable than the interaction between the center block and the two outer blocks, hence, morphologies with a/c interfaces are greatly suppressed.

Figure 4a shows the phase diagram of a system for

which $\gamma_1 = 1$ and $\gamma_2 = 0.2$. In particular, for a symmetric diblock copolymer, where $f_a = f_c$ and $\gamma_1 = 1$, the phase diagram shows that the transition from the lamellar to the lamella–cylinder phase occurs at $f_b = 0.35$ and that the transition from the lamella–cylinder to the lamella–sphere occurs at $f_b = 0.17$. These results qualitatively agree with those in a recent paper by Stadler et al.,[24] who studied the morphologies of *symmetric triblock copolymers* by using the Meier/Alexander/de Gennes/Semenov approach. However, their calculation also shows a stable cylinder–ring phase when γ_2 is reduced to 0.1. This result is puzzling in view of the architectural symmetry of the symmetric triblock copolymer and the obvious microstructural asymmetry of the cylinder–ring phase.

We show in Figure 4b a phase diagram of symmetric triblock copolymers in terms of f_b and γ_2 for transitions from the lamellar, to the lamella–cylinder, and then to lamella–sphere phases. It is clear that the regions for the lamella–cylinder and lamella–sphere phases are greatly enlarged when γ_2 is reduced.

To study the influence of γ_1 on the morphology of triblock copolymers, we fix γ_2 at some large value. Under the assumption that $\sigma_{ab} \leq \sigma_{bc}$, the system can be classified into two types: $\gamma_1 = \sigma_{bc}/\sigma_{ab} = 1$ or $\gamma_1 = \sigma_{bc}/\sigma_{ab} > 1$. For $\gamma_1 = 1$, the morphology of the system remains unchanged when the volume fraction of blocks a and c are exchanged. It is a common feature of systems with $\gamma_1 = 1$ that the three-component triangle phase diagrams have a reflection symmetry with respect to the vertical line $f_a = f_c$. The reflection symmetry disappears when $\gamma_1 \neq 1$. When $\gamma_1 > 1$, i.e., the interfacial tension $\sigma_{bc} > \sigma_{ab}$, near the edge ab, the system can achieve a low interfacial energy by forming a coaxial cylinder phase, with c blocks forming the inner cylinder, b blocks forming the shell, and a being the matrix. In Figure 5a, the phase diagram of a system with $\gamma_1 = 2.0$ and $\gamma_2 = 5.0$ is presented, and the region of the coaxial cylinder phase near the edge ab of the phase diagram is greatly enlarged in comparison with that in Figure 3a. Figure 5b shows the free energies of the lamellar, coaxial cylinder, and cylinder–sphere phases as γ_1 varies, with $f_a = 0.8$, $f_c = 0.1$, and $\gamma_2 = 5.0$. When $\gamma_1 > 1.55$, the coaxial cylinder phase becomes the stable state. However, the cylinder–sphere phase remains nearly stable in Figure 5b. The cylinder–sphere phase becomes stable only when an additional condition $f_c/f_b \ll 1.0$ is satisfied. Figure 5c shows the free energies of the lamellar, coaxial cylinder, and cylinder–sphere phases as a function of f_c at $\gamma_1 = 2.0$, $\gamma_2 = 5.0$, and $f_a = 0.8$. The cylinder–sphere phase is the stable phase when $f_c < 0.046$, i.e., $f_c/f_b < 0.3$. Therefore, the relative stability of the coaxial cylinder phase and cylinder–sphere phase is enhanced when γ_1 increases.

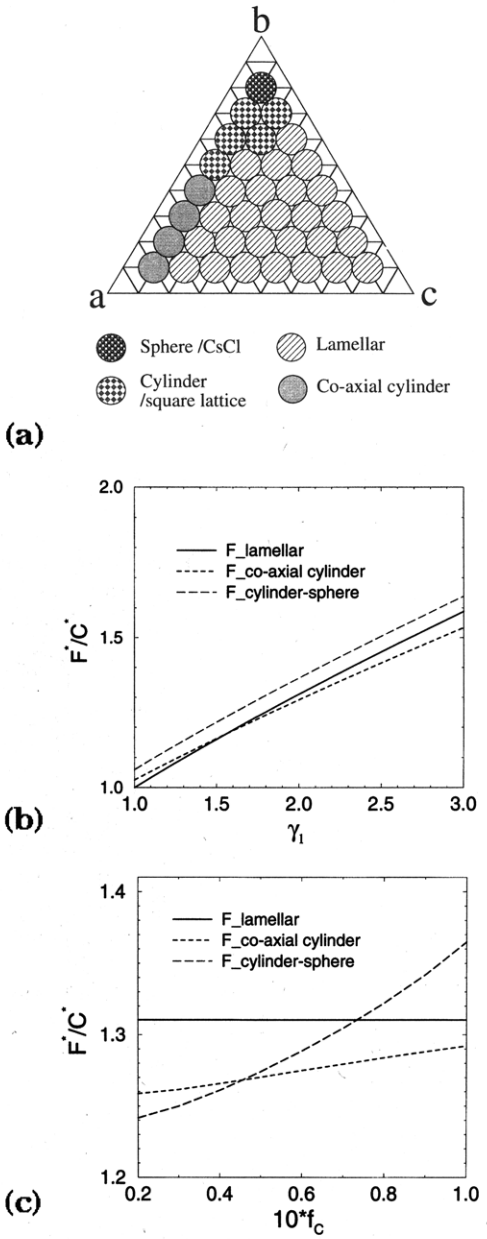

Figure 5. (a) Phase diagram for $\gamma_1 = 2.0$ and $\gamma_2 = 5.0$. (b) Equilibrium free energy F^*/C^* for the lamellar, coaxial cylinder, and cylinder–sphere phases as a function of γ_1 at volume fractions $f_a = 0.8$ and $f_c = 0.1$ and $\gamma_2 = 5.0$. (c) Equilibrium free energy F^*/C^* for the lamellar, coaxial cylinder, and cylinder–sphere phases as a function of f_c at fixed $f_a = 0.8$ and $\gamma_1 = 2.0$ and $\gamma_2 = 5.0$.

IV. Discussion

A theoretical understanding of the effect of volume fractions and the various interfacial tensions on the morphology of triblock copolymers enables us to predict and explain a variety of structures that can be formed by these systems. We now discuss several interesting experimental results in light of our calculated phase diagrams.

In a series of experiments by Auschra et al.,[28,29] the lamella–cylinder, lamella–sphere, and cylinder–ring phases were discovered for the first time. Using poly(styrene-*b*-ethylene-*co*-1-butene-*b*-methacrylate) (P(S-*b*-EB-*b*-MMA)) triblock copolymers, they demonstrated that the lamellar phase was formed at the composition 0.24/0.38/0.38, the lamella–cylinder phase was formed at 0.48/0.17/0.35, and the cylinder–ring phase was formed at 0.45/0.06/0.49. The literature data for the interfacial tensions between the components of P(S-*b*-EB-*b*-MMA) are given in Table 2.[35]

Table 2

	PS/PMMA	PS/PEB	PEB/PMMA
σ (150 °C)/(dyn cm^{-1})	1.5	5.0	9.5

If we denote "A" as PS, "B" as PEB, and "C" as PMMA, their relative interfacial tensions are $\gamma_2 = \sigma_{AC}/\sigma_{AB} = 0.3$ and $\gamma_1 = \sigma_{BC}/\sigma_{AB} = 1.9$. The system consisting of P(S-*b*-EB-*b*-MMA) belongs to the first type in the second row of Table 1. Figure 6a is our calculated phase diagram of such A–B–C copolymers. The phase diagram indi-

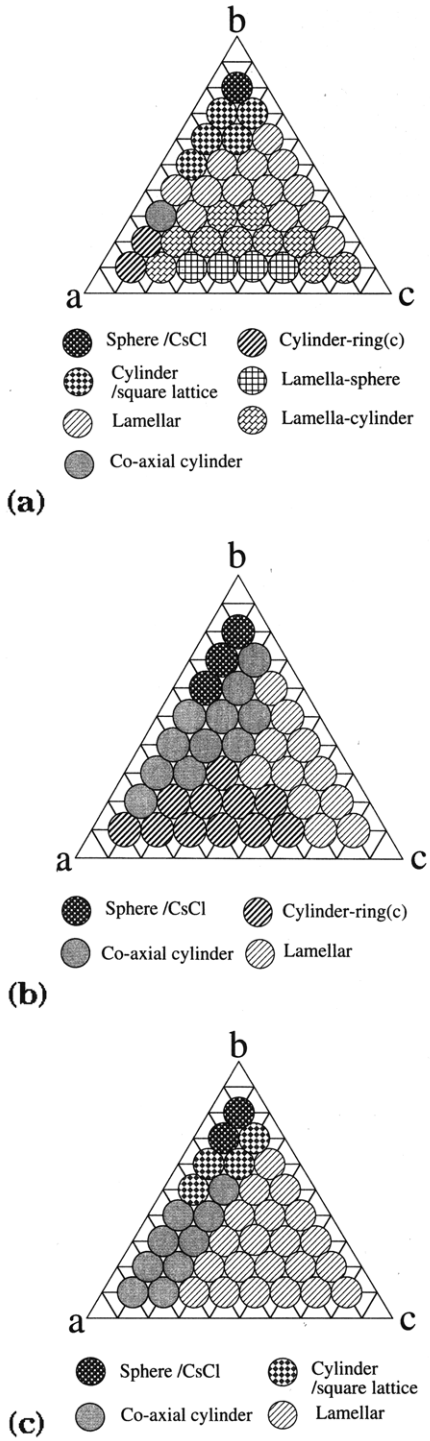

Figure 6. (a) Phase diagram of the P(S-*b*-EB-*b*-MMA) system of which $\gamma_1 = 1.9$ and $\gamma_2 = 0.3$. (b) Phase diagram of the P(S-*b*-MMA-*b*-EB) system of which $\gamma_1 = 6.33$ and $\gamma_2 = 3.33$. (c) Phase diagram of the P(MMA-*b*-S-*b*-EB) system of which $\gamma_1 = 3.33$ and $\gamma_2 = 6.33$.

cates that the system is in the lamellar phase at the composition 0.24/0.38/0.38 and in the lamella–cylinder phase at 0.48/0.17/0.35; both are consistent with the experimental results of Auschra et al.[28] However, there is a notable discrepancy at 0.45/0.06/0.49. Our calculation predicts that the system should be in the lamella–sphere phase, while a cylinder–ring phase was observed experimentally by Auschra et al. From Figure 6a, it is clear that the cylinder–ring phase with C blocks forming the cylinder can appear only at the corner of a where $f_b < 0.3$ and $f_c < 0.2$. Although our free energy calculation is approximate, we do not believe that the error due to the approximation can be large enough to lead to this discrepancy. It should also be noted that our calculations predict that cylinder–ring domains on a hexagonal lattice always have a lower energy than those on a square lattice.

Parts b and c of Figure 6 show the phase diagrams of P(S-*b*-MMA-*b*-EB) and P(EB-*b*-S-*b*-MMA), simply designated as A–C–B and B–C–A, respectively. Using the definition of γ_2 and γ_1, the system consisting of A–C–B has the relative interfacial tensions $\gamma_2 = 3.33$ and $\gamma_1 = 6.33$, and B–A–C has the relative interfacial tensions $\gamma_2 = 6.33$ and $\gamma_1 = 3.33$, which belong to the second and third in the second row of Table 1. It is obvious that switching the sequences of the three blocks leads to very different structures of the phase diagrams.

Another interesting experimental observation can also be explained and the relative interfacial tension of the system can be estimated by the understanding of the effect of γ_2 and γ_1 on the morphology of triblock copolymers. Mogi et al.[25] observed a lamellar phase in 1:1:1 P(isoprene-*b*-styrene-*b*-2-vinylpyridine) (ISP) triblock copolymers, whereas a coaxial cylinder phase of P and I in an S matrix was found in P(S-*b*-I-*b*-P) by Gido et al.[26] Our free energy calculation of the lamellar and the coaxial cylinder phases shows that when $\sigma_{bc}/\sigma_{ab} \geq 4.3$, the coaxial cylinder phase, with C forming the inner cylinders, is the stable phase. The fact that the lamellar phase was formed at 1:1:1 of P(I-*b*-S-*b*-P) indicates that $1/4.3 < \sigma_{IS}/\sigma_{SP} < 4.3$. On the other hand, the fact that the coaxial cylinders formed in 1:1:1 of SIP indicated that $\sigma_{IP}/\sigma_{IS} > 4.3$. These results enable us to bracket the range of the relative interfacial tensions for I, S, and P.

V. Conclusions

In this paper, we have presented a systematic study of the rich and fascinating morphologies that can form in ABC triblock copolymers in the strong segregation limit. Our results demonstrate the crucial dependence of the phase behavior of an ABC triblock copolymer system on the sequencing of the three blocks. The effects of the interaction parameters have also been investigated. In contrast to the AB diblock copolymers where, in the strong segregation limit, the morphology is determined uniquely by the composition, the relative strengths of the interaction parameters in a triblock copolymer system affect the morphology phase diagrams in a significant way.

Our calculation has made use of an approximation proposed by Ohta and Kawasaki in which the chain conformation free energy is approximated by a Coulomb-like interaction. Because of this approximation, our phase diagrams can only be considered as qualitatively correct. However, the quantitative accuracy of this approximation may not be as poor as it appears to be. Since the calculation of the phase diagrams involves taking the difference between the free energies of the different ordered phases, it is possible that the errors caused by this approximation may cancel to some extent.

Another (technical) approximation involves our representation of the ordered structures, in that we only considered domains with uniform curvature. In reality, the cylinders and spheres are deformed due to the lattice structures in which they are embedded. Allowing this deformation will lead to lower free energies for structures involving curved domains relative to the lamellar structure, hence increasing the stability of these phases.

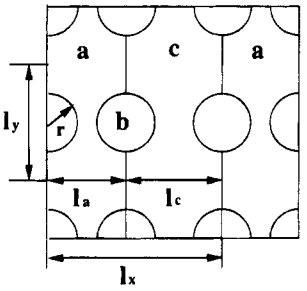

Figure 7. Cross-sectional view of the lamella–cylinder phase (see also Figure 2c). l_x and l_y are the primitive vectors in the xy plane, l_a and l_c are the thicknesses of the a and c domains, respectively, and r is the radius of the cylinder containing the b blocks.

In spite of these approximations, our calculation does seem to have captured many of the essential features of the ABC triblock copolymer systems in the strong segregation limit. Our results compare favorably with experimental observations. In addition, we have predicted the existence of some new structures: the lamella–cylinder–II phase, the lamella–sphere–II phase, and the cylinder–sphere phase; it will be of interest to observe these new phases experimentally. It is hoped that this study provides a systematic (although crude) guide for future experiments and more refined theories of the morphology of ABC triblock copolymers.

Appendix

In this Appendix, we present the details of the free energy calculation for the lamella–cylinder phase to illustrate the method that has been used. The calculation of other morphologies which are considered in determining the lowest free energy in the phase diagrams is carried out in a similar way. Instead of presenting the detailed calculations of their free energy, we only provide their schematic representations in Figure 2.

The lamella–cylinder phase was first discovered by Auschra et al.[28] A schematic representation of this structure is given in Figure 2c.

We choose our coordinate system such that the cylinder axis in the lamella–cylinder structure is oriented in the $\hat{z}$ direction. In the xy plane, the primitive vectors are $l_x\hat{x}$ and $l_y\hat{y}$. The thickness of the a and c domains are l_a and l_c, respectively, and r is the radius of the cylinders containing the b blocks, as shown in Figure 7. For simplicity, we have assumed that the half circles containing blocks b in a domains and c domains have the same curvature. The reciprocal lattice vectors are given by

$$\vec{Q} = \frac{2\pi}{l_x}m_1\vec{e}_x + \frac{2\pi}{l_y}m_2\vec{e}_y \tag{A1}$$

with m_1 and m_2 being integers. The unit cell has been chosen as shown in Figure 7 with unit cell volume V_{cell} equal to $l_x l_y L$.

The form factor of a domain and c are given by

$$\Psi_a(Q) = \exp\{iQ_x l_a/2\}\Psi'_A(Q) \tag{A2}$$

$$\Psi_c(Q) = \exp\{-iQ_x l_c/2\}\Psi'_C(Q) \tag{A3}$$

where $\Psi'_a(Q)$ and $\Psi'_c(Q)$ are given by

$$\Psi'_\alpha(Q) = \frac{4L}{V_{cell}}\int_0^{l_a/2} dx \int_{Y_\alpha(x)}^{l_y/2} dy \cos(Q_x x)\cos(Q_y y) \tag{A4}$$

with

$$Y_\alpha(x) = \begin{cases} 0 & (0 \le x \le l_\alpha/2 - r) \\ [r^2 - (x - l_\alpha/2)^2]^{1/2} & (l_\alpha/2 - r \le x \le l_\alpha) \end{cases} \tag{A5}$$

with α = a, c.

The form factors can be evaluated numerically. We choose l_x as the characteristic length scale l and scale Q, l_a, l_c, l_y, and r in eqs A2–A5 by l_x. The scaled variables $\hat{l}_a$, $\hat{l}_c$, $\hat{l}_y$, and $\hat{r}$ are not independent of each other, but are related by the equations:

$$\hat{l}_a + \hat{l}_c = 1 \tag{A6}$$

$$\hat{l}_a - \pi\hat{r}^2/\hat{l}_y = f_a \tag{A7}$$

$$2\pi\hat{r}^2/\hat{l}_y = 1 - f_a - f_c \tag{A8}$$

Equations A7 and A8 arise from the constraint that the volume fractions of a and c in a unit cell are f_a and f_c, respectively. Thus, we have

$$\hat{l}_a = f_a + \frac{1}{2}(1 - f_a - f_c) \tag{A9}$$

$$\hat{l}_c = \frac{1}{2}(1 - f_a - f_c) \tag{A10}$$

$$\hat{r} = [\hat{l}_y(1 - f_a - f_c)/2\pi]^{1/2} \tag{A11}$$

Substituting eqs A9–A11 to eq 1, we have the long-range part of the free energy F_L

$$F_L = \frac{l^2}{2N}\Phi(f_a, f_c; \hat{l}_y) \tag{A12}$$

where

$$\Phi(f_a, f_c; \hat{l}_y) = \sum_{\hat{Q}} \frac{1}{\hat{Q}^2}(A_L^{aa}(f_a, f_c)\,\Psi'_a(\hat{Q})^2 + A_L^{cc}(f_a, f_c)\,\Psi'_c(\hat{Q})^2 + 2\cos(\hat{Q}_x/2)\,A_L^{ac}(f_a, f_c)\,\Psi'_a(\hat{Q})\,\Psi'_c(\hat{Q}))$$

with $\hat{Q}_x = Q_x l$.

The short-range part of the free energy is given by

$$F_S = \sigma_{av} v_0 N/l \tag{A13}$$

where

$$\sigma_{av} = [(\sigma_{ab} + \sigma_{bc})2\pi\hat{r} + 2\sigma_{ac}(\hat{l}_y - 2\hat{r})]/\hat{l}_y \tag{A14}$$

Substituting $\Phi(f_a, f_c; \hat{l}_y)$ and σ_{av} in eq 10, we can obtain F^*. Since $\Phi(f_a, f_c; \hat{l}_y)$ and σ_{av} are both functions of $\hat{l}_y$, which is the ratio of the two characteristic length scales l_x and l_y, the mininum free energy of the lamella–cylinder–I phase can be obtained by numerically minimizing F^* with respect to $\hat{l}_y$.

Acknowledgment. We thank Julia A. Kornfield for helpful discussions. This research is supported in part by donors of the Petroleum Research Fund, adminis-

tered by the American Chemical Society, and by the National Science Foundation (Grant No. ASC-9217368).

References and Notes

(1) Morkved, T. L.; Wiltzius, P.; Jaege, H. M.; Grier, D. C.; Witten, T. A. *Appl. Phys. Lett.* **1994**, *64*, 422.
(2) Kirk, W. P., Reed, M. A., Eds. *Nanostructures and Mesoscopic Systems;* Academic: New York, 1992.
(3) Archibald, D. D.; Mann, S. *Nature* **1993**, *364*, 430.
(4) Kresge, C. T.; Leonowitcz, M. E.; Roth, W. J.; Vartuli, J. C.; Beck, J. S. *Nature* **1992**, *359*, 710.
(5) Helfand, E.; Wasserman, Z. R. *Macrmolecules* **1980**, *13*, 994 and earlier references cited therein.
(6) Semenov, A. N. *Sov. Phys. JETP* **1985**, *61*, 733.
(7) Ohta, T.; Kawasaki, K. *Macromolecules* **1986**, *19*, 2621.
(8) Ohta, T.; Kawasaki, K. *Macromolecules* **1990**, *23*, 2413.
(9) Leibler, L. *Macromolecules* **1980**, *13*, 1602.
(10) Fredrickson, G. H.; Helfand, E. *J. Chem. Phys.* **1987**, *87*, 697.
(11) Brazovskii, A. *Soc. Phys. JETP* **1975**, *41*, 85.
(12) Hong, K. M.; Noolandi, J. *Macromolecules* **1981**, *14*, 727; **1981**, *14*, 736. Hong, K. M.; Noolandi, J. *Macromolecules* **1982**, *15*, 482; **1984**, *17*, 1531. Whitmore, M. D.; Noolandi, J. *Macromolecules* **1988**, *21*, 2972.
(13) Muthukumar, M.; Melenkevitz, J. *Macromolecules* **1991**, *24*, 4199.
(14) Muthukumar, M. *Macromolecules* **1993**, *26*, 5259.
(15) Matsen, M. W.; Schick, M. *Phys. Rev. Lett.* **1994**, *72*, 2660.
(16) Olmsted, P. D.; Milner, S. T. *Phys. Rev. L* **1994**, *72*, 936; **1995**, *74*, 829.
(17) Bates, F. S.; Fredrickson, G. H. *Annu. Rev. Phys. Chem.* **1990**, *41*, 525.
(18) Likhtman, A. E.; Semenov, A. N. *Macromolecules* **1994**, *27*, 3103.
(19) Anderson, D. M.; Thomas, E. L. *Macromolecules* **1988**, *21*, 3221.
(20) Hajduk, D. A.; Harper, P. E.; Gruner, S. M.; Honecker, C. C.; Kim, G.; Thomas, E. L.; Fetters, L. J. *Macromolecules* **1994**, *27*, 4063.
(21) Nakazawa, H.; Ohta, T. *Macromolecules* **1993**, *26*, 5503.
(22) Riess, G. In *Thermoplastic Elastomers. A Comprehensive Review;* Ledge, N. R., Holden, G., Schroeder, H. E., Eds.; Hanser: Munich, 1987; Chapter 12.2, p 325.
(23) Riess, G.; Schlienger, M.; Marti, S. *J. Macromol. Sci. Phys.* **1989**, *B17* (2), 355.
(24) Stadler, R.; Auschra, C.; Beckmann, J.; Krappe, U.; Voigt-Martin, I.; Leibler, L. *Macromolecules* **1995**, *28*, 3080–3097. This paper appeared after we submitted our manuscript.
(25) Mogi, Y.; Kotsuji, H.; Kaneko, Y.; Mori, K.; Matsushita, Y.; Noda, I. *Macromolecules* **1992**, *25*, 5408. Mogi, Y.; Mori, K.; Matsushita, Y.; Noda, I. *Macromolecules* **1992**, *25*, 5412. Mogi, Y.; Mori, K.; Kotsuji, H.; Matsushita, Y.; Noda, I. *Macromolecules* **1993**, *26*, 5169.
(26) Gido, S. P.; Schwark, D. W.; Thomas, E. L.; Goncalves, M. D. *Macromolecules* **1993**, *26*, 2636.
(27) Matsushita, Y.; Tamura, M.; Noada, I. *Macromolecules* **1994**, *27*, 3680.
(28) Auschra, C.; Stadler, R. *Macromolecules* **1993**, *26*, 2171.
(29) Beckmann, J.; Auschra, C.; Stadler, R. *Macromol. Rapid Commun.* **1994**, *15*, 67.
(30) Stillinger, F. H. *J. Chem. Phys.* **1982**, *78*, 4654.
(31) Wu, D.; Chandler, D.; Smit, B. *J. Phys. Chem.* **1992**, *96*, 4077. Deem, M. W.; Chandler, D. *Phys. Rev. E* **1994**, *49*, 4276 and 4268.
(32) Kane, L.; Spontak, R. J. *Macromolecules* **1994**, *27*, 1267.
(33) Helfand, E.; Tagami, Y. *J. Polym. Sci.* **1971**, *B9*, 741; *J. Chem. Phys.* **1971**, *56*, 3592; **1972**, 1812.
(34) Zheng, W.; Wang, Z.-G., unpublished results.
(35) *Polymer Handbook,* 3rd ed.; Brandrup, J., Immergut, E. H., Eds.; John Wiley & Sons: New York, 1989.

MA950489U